ACS central science

Research Article

http://pubs.acs.org/journal/acscii

Reversible Self-Assembled Monolayers (rSAMs): Adaptable Surfaces for Enhanced Multivalent Interactions and Ultrasensitive Virus Detection

Sing Yee Yeung,[†] Annabell Mucha,[‡] Ravindra Deshmukh,[‡] Malak Boutrus,[‡] Thomas Arnebrant,[†] and Börje Sellergren*[,†,‡]

[†]Department of Biomedical Sciences and Biofilms-Research Center for Biointerfaces (BRCB), Faculty of Health and Society, Malmö University, 20506 Malmö, Sweden

[‡]Faculty of Chemistry, Technical University of Dortmund, Dortmund, 44227 Germany

Supporting Information

ABSTRACT: We report on the design of pH-switchable monolayers allowing a reversible and ordered introduction of affinity reagents on sensor surfaces. The principal layer building blocks consist of α-(4-amidinophenoxy)alkanes decorated at the ω-position with affinity ligands. These spontaneously self-assemble on top of carboxylic acid terminated SAMs to form reversible homo or mixed monolayers (rSAMs) that are tunable with respect to the nature of the head group, layer order and stability while featuring pH responsiveness and the dynamic nature of noncovalent build assemblies. We show that this results in a range of unique biosensor features. As a first example a sialic acid rSAM featuring strong lectin affinity is here used to sense hemagglutinin and influenza virus (H5N1) at the pM and fM level by in situ ellipsometry in a fully reversible fashion. We believe that the rSAM concept will find widespread use in surface chemistry and overall for boosting sensitivity in affinity biosensors.

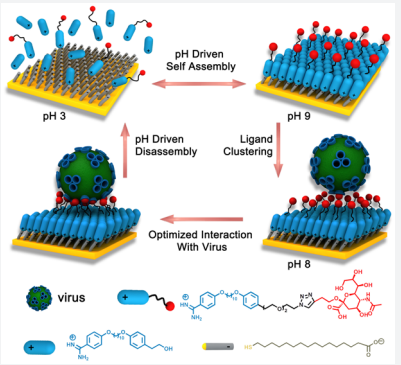

Pathogenic virus strains pose a major threat to human health.[1,2] Recent disease outbreaks highlight the need for fast, simple, and reliable tests for detecting such viruses, e.g., for surveillance, clinical diagnosis, or screening of drug candidates and vaccines.[3,4] Of particular urgency is the realization of practical sensors capable of rapid typing and subtyping of influenza virus strains. Whereas antibodies and aptamers are effective virus receptors offering excellent specificity for virus subtypes, biomimetic sensors employing glycans as recognition elements offer distinct advantages in this regard.[5−10] The design of these sensors is inspired by the strong multivalent lectin−glycan interactions occurring between influenza viruses and their corresponding hosts.[11,12] Hence, several multivalent formats presenting sialic acids such as synthetic inhibitors,[13,14] polymers,[15] lipid bilayers,[16] liposomes,[5,17] self-assembled monolayers (SAMs),[8,10] and nanoparticles[12,18] have been shown to exhibit enhanced affinity as compared to singular interactions. With the exception of systems comprising fluid layers such as liposomes and lipid bilayers, these binders build on scaffolds covalently interconnecting the glycans. This confinement may sterically impede their binding to multivalent targets in a way that is absent in dynamic biological membrane mimics. Two dimensional fluidic alternatives such as the lipid bilayers are on the other hand fragile and unstable under atmospheric conditions, rendering them unsuitable for robust biosensing.[19] This highlights the need for molecular architectures that combine robustness with the dynamic nature of cellular membranes.

We have previously reported on reversible self-assembled monolayers (rSAMs) of α,ω-bis(4-amidinophenoxy)alkanes and their use as a switchable platform for molecular recognition.[20−23] As for traditional SAMs of alkanethiolates on gold, rSAMs are tunable with respect to the layer order and stability, but, in contrast to the former, rSAMs feature reversibility and the dynamic nature of noncovalent build assemblies. The bis-benzamidines spontaneously assemble in neutral or alkaline aqueous solution on carboxylic acid terminated thiol SAMs to form ordered monolayers with tunable pH responsiveness. Layer thickness and order correlate with the molecular length of the amphiphile. Thus, beyond a certain length the layers feature crystalline order and an odd even chain length related tendency for bilayer formation.[21] These layers are stable toward rinsing and resist exchange by plasma proteins and charged surfactants. The amidine functional rSAMs display furthermore a charge selective affinity for proteins,[20] oligonucleotides,[22] sugar phosphates,[23] and cofactors[23] and can be restored by a simple pH cycle.

Recently our aim has been to extend the rSAM repertoire to allow introduction of any optional headgroup in an ordered but reversible fashion. Applications of such systems in areas currently associated with SAMs of chemisorbed molecules can be envisaged.[8,10,24,25] For instance, ligands featuring lateral mobility can adapt to the presence of a given target receptor thereby providing multivalent interactions and enhanced binding affinity (Figure 1B). We will

Received: September 5, 2017
Published: November 10, 2017

DOI: 10.1021/acscentsci.7b00412
ACS Cent. Sci. 2017, 3, 1198−1207

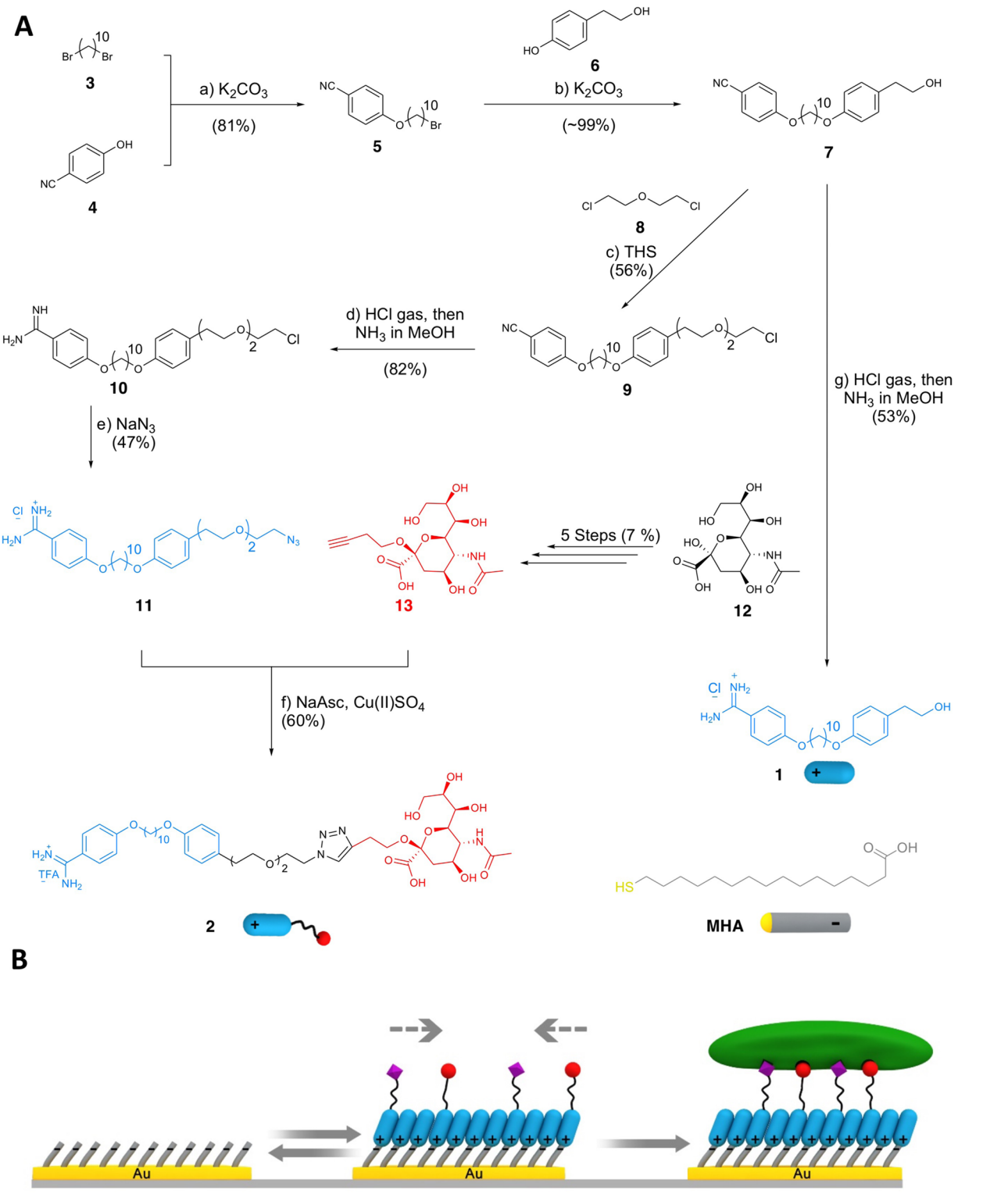

Figure 1. (A) Synthetic pathway of OH-terminated amphiphile **1** and sialic acid terminated amphiphile **2** and (B) use of **1** and **2** to form an adaptable rSAM. Reagents and conditions in panel A: (a) 1,10-dibromodecane **3** 10 equiv, K_2CO_3 2 equiv, acetone, 80 °C, 24 h, 81%; (b) 4-(2-hydroxyethyl)phenol **6** 2.0 equiv, K_2CO_3 2.0 equiv, acetone, 80 °C, 24 h, ~99%; (c) 2-chloroethyl ether **8** 43 equiv, tetrabutylammonium hydrogen sulfate (THS) 2.0 equiv, NaOH solution (50% w/w), rt, 18 h, 56%; (d) HCl gas, MeOH, 0 °C → rt, 24 h, then NH_3 in MeOH, rt, 24 h, 82%; (e) NaN_3 4.0 equiv, DMF, 90 °C, 24 h, 47%; (f) NaAsc 3.0 equiv, Cu(II)SO_4 0.3 equiv, H_2O/2-butanol (1:2), rt, 4 h, 60%; (g) HCl gas, 1,4-dioxane, MeOH, 0 °C → rt, 24 h, then NH_3 in MeOH, rt, 24 h, 53%.

show that this results in a range of unique features with relevance to biosensing, multivalent molecular recognition, and pathogen detection. Here we report on a sialic acid rSAM featuring strongly enhanced lectin affinity. The synthesis of the layer components, their self-assembly on modified gold, and the structure and order of such layers will be described. Finally the use of the concept to sense influenza virus (H5N1) at the ultratrace level in a reversible fashion will be shown.

DOI: 10.1021/acscentsci.7b00412
ACS Cent. Sci. 2017, 3, 1198−1207

RESULTS AND DISCUSSIONS

Design and Synthesis. We have previously shown that α,ω-bis(4-amidinophenoxy)alkanes form mono- and bilayers on carboxylic acid terminated alkanethiols, preassembled on gold. Layer order increased with alkane chain length and crystalline order was observed for layers formed from molecules with chains exceeding 7 carbons.[20,21] In order to extend the rSAM concept from homo- to heterodifunctionalized amphiphiles we aimed at appending biologically active ligands at their ω-position. The design of such surfaces requires attention to the geometrical constraints governing the receptor−ligand interactions.[11,12] Critical parameters are the surface density of ligands, the flexibility and polarity of the spacer, and the distance separating the ligand from the underlying surface of the SAM. Mixed SAMs,[8,25] polymers,[15] or liposomes[17,26] have been extensively studied for this purpose. Binary mixtures of amphiphiles typically containing 1−20% of sialic acid terminated amphiphile have proven optimal for inhibiting agglutination or infection or for sensing.[8] Accessibility to lectin binding is promoted by inserting spacers of 2−3 ethylene glycol repeat units between the glycan and the SAM or liposome surface.[5,11,12,26] Taking these criteria into consideration we designed a convergent synthesis strategy (Figure 1) ending in the alkyne sialic acid **13** and the azide-terminated amidine fragment **11** which were joined by a final Sharpless/Huisgen click coupling[27] to afford **2**. Preceding the coupling, **11** was prepared in five steps by sequential Williamson ether synthesis followed by Pinner conversion[28] and azide substitution[29] in an overall yield of 17%. The α alkyne sialic acid **13** was synthesized in five steps as recently reported[30] whereas **1** was obtained by direct Pinner conversion of **7**. In order to compare the rSAMs with a static chemisorbed SAM we also synthesized amino-spacer modified sialic acid **14** (Supporting Information section 1.6) serving to covalently tether sialic acid to a SAM of MHA.

In Situ Ellipsometry. To confirm formation, structure, and properties of adsorbed films we used in situ ellipsometry, IRAS, contact angle, and AFM as outlined in Supporting Information Figure 1. In general in situ ellipsometry data are evaluated based on changes in the angles Δ and Ψ, which can be used to calculate the change in thickness and mass of a thin film in real time.

The technique was first used to verify formation of the thiol SAM used as rSAM anchor. We have previously shown that ordered SAMs of the long chain alkanoic acid MHA on gold are well suited for this purpose.[20,21] The results (Supporting Information Figure 2, Supporting Information Table 1) collectively agree with previous findings which support a fast spontaneous assembly resulting in ordered monolayers with the alkane chains slightly tilted with respect to the surface normal.[31]

We then investigated the adsorption mode of the amidine amphiphiles **1** and **2** alone or as mixtures on this SAM. Figure 2A shows the average film thickness and amount adsorbed during adsorption of the amphiphiles from 50 μM solutions in pH 9 sodium borate buffer.

The adsorption kinetics, the limiting film thickness, and the stability to rinsing depended strongly on the type of amphiphile system. Considering first OH terminated amphiphile **1**, this showed a relatively slow adsorption while forming a stable film with a thickness of 46 Å, hence exceeding the amphiphile molecular length (28 Å) assuming an extended chain conformation (Supporting Information Table 1). This agrees with our previous study of the adsorption mode of a homologous series of bis-benzamidines on negatively charged surfaces[20] and indicates formation of bilayered structures featuring an underlying layer of high order and a less ordered top layer. In contrast, **2** displayed a very fast adsorption and a final film thickness of 54 Å prior to rinsing, exceeding only slightly the theoretical value of 47 Å. The layer thickness dropped significantly upon rinsing with pH 8 buffer leveling off at 19 Å. As seen in Figure 2B, this layer can be rapidly destabilized/restabilized by cycling the pH between 3 and 9, showing that the process is fully reversible.

The contrasting behavior of these amphiphiles is likely related to their water solubility. **2** with its hydrophilic carbohydrate headgroup is highly water-soluble, and we anticipate a SAM with a low surface energy with respect to the borate buffer media. This stabilizing contribution is however counteracted by the bulkiness of the headgroup, which together with charge repulsion likely hinders close packing of the amphiphile chains and hence an ordered monolayer to form. OH-terminated **1** is on the other hand poorly water-soluble and may therefore adsorb in the form of aggregates: this can explain the slower adsorption kinetics and formation of bilayered structures. We therefore went on to study a mixed rSAM. Adsorption in the presence of a mixture of the two amphiphiles **1** and **2** (χ_2 = 0.2) occurred at a rate that was intermediate between those of **1** and **2** alone. The resulting layer featured a film thickness close to that of **2** alone, but, in contrast to the latter, this layer was completely stable to rinsing. The data supports the formation of a mixed assembly but does not offer any insight into the structure of the films and stoichiometry of the layer components.

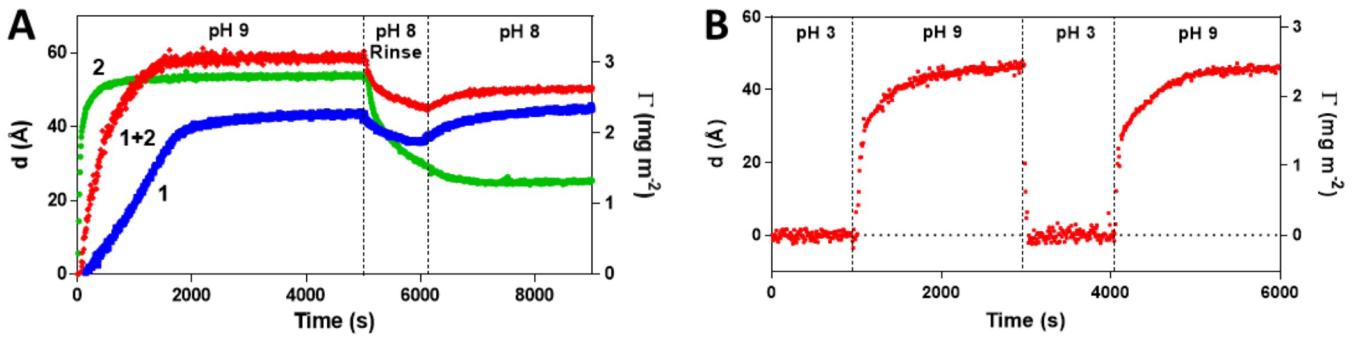

Figure 2. (A) Film thickness, *d*, and amount adsorbed, Γ, estimated by in situ ellipsometry, versus time during adsorption of **1** (blue trace), **2** (green trace), or a mixture of **1** and **2** (χ_2 = 0.2) (red trace) (50 μM in buffer) on MHA modified gold at pH 9. Thickness values after pH 9 adsorption, d_{ads} (Å), and after rinsing in pH 8 buffer, d_{rinse} (Å), are tabulated in Supporting Information Table 1. (B) Film thickness, *d*, and amount adsorbed, Γ, measured during the pH-driven self-assembly of **2** on MHA modified gold at pH 9 followed by cycling the pH between 9 and 3 in borate buffer (0.01 M). The desired pH was adjusted using 0.1 M NaOH or 0.1 M HCl solution in a discontinuous system.

DOI: 10.1021/acscentsci.7b00412
ACS Cent. Sci. 2017, 3, 1198−1207

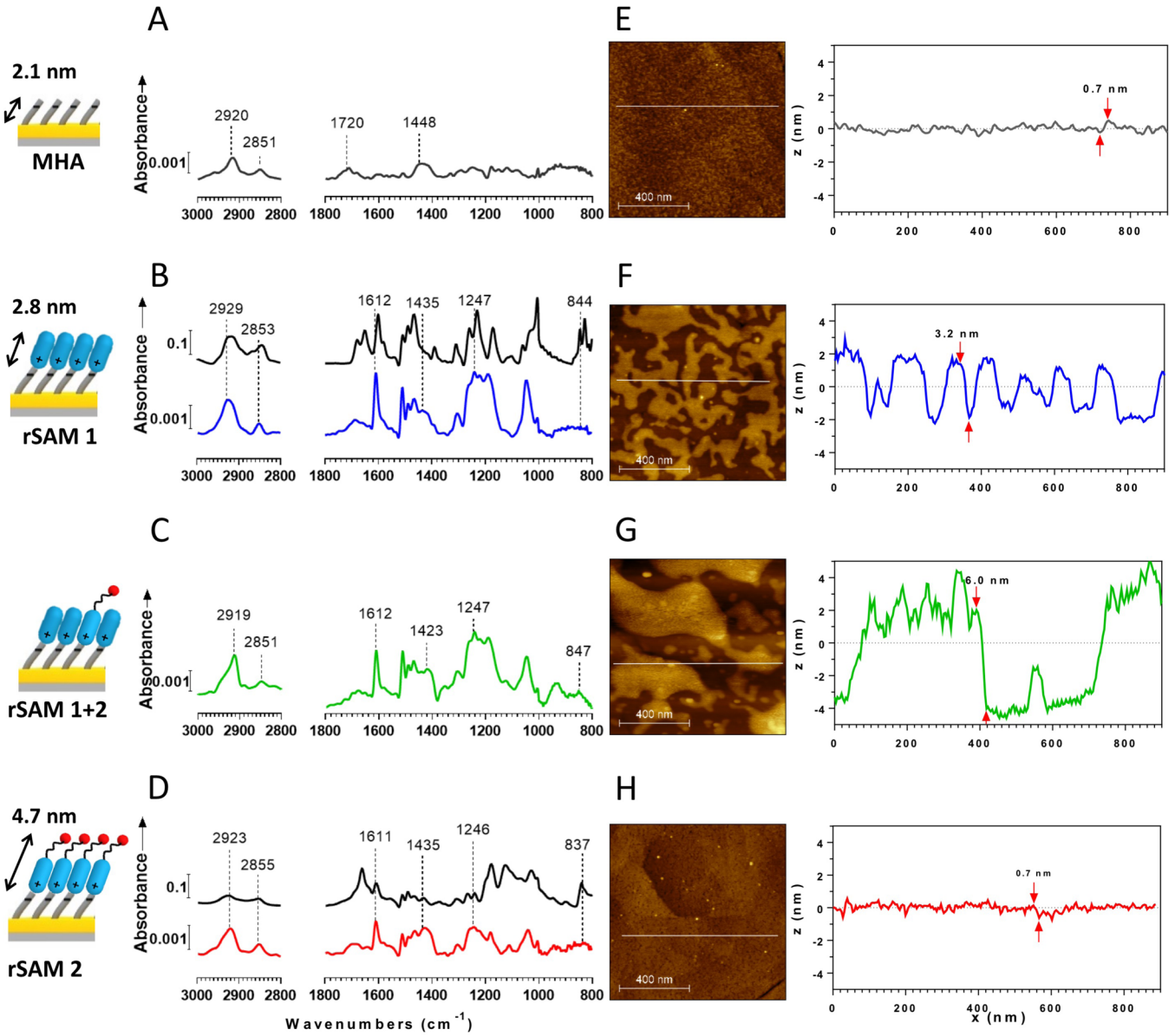

Figure 3. (A–D) Baseline-corrected IR reflection–absorption (IRAS) spectra of (A) MHA on gold, (B) rSAM-**1** (lower blue trace), (C) rSAM-**1**+**2** (green trace), and (D) rSAM-**2** (lower red trace). The black traces in panels B and D correspond to spectra of bulk **1** and **2** in their salt forms. (E–H) Topographical atomic force microscopy (AFM) images (1 μm × 1 μm) of (E) a SAM of MHA on a gold–mica surface, (F) rSAM-**1**, (G) rSAM-**1**+**2**, and (H) rSAM-**2**. The images were obtained in quantitative nanoscale mechanical (QNM) mode in air. The height differences between valley and peak are obtained from a section analysis as indicated by red arrows.

IRAS and AFM. To obtain further insight into the nature of these films we used infrared reflection absorption spectroscopy (IRAS) and atomic force microscopy (AFM). All IRAS spectra were compared with the attenuated total reflectance (ATR) spectra of the corresponding bulk samples in order to draw conclusions concerning layer stoichiometry and the order and orientation of the amphiphile molecules. As an example, Figure 3 shows the spectra of rSAMs and a SAM of MHA on gold together with the ATR spectrum of their respective hydrochloride and trifluoroacetate salt forms. Inspection of the spectra of the modified MHA-SAMs leads to identification of all significant peaks present in the ATR spectrum (see Supporting Information Tables 2 and 3 for assignments). This provides evidence for the presence of the amidines on the acid monolayer. Compared to the ATR spectra, however, the spectra of the rSAMs exhibit different relative band intensities and bandwidths which are informative about the order and orientation of the layer components. Particularly striking are the relative intensities of the benzene $(C{=}C)_{1,4}$ stretch at 1611 cm^{-1} and the C–O–C asymmetric stretch at 1247 cm^{-1} relative to the intensities of the aromatic C–H out-of-plane bending mode at 841 cm^{-1} and the amidine N–C=N asymmetric stretch found around 1690 cm^{-1}, the latter coinciding with the amide I and C=O stretch of the sialic acid headgroup. The former two bands have transition dipole vectors oriented along the 1,4-axis of the benzene ring and the longitudinal axis of the alkyl chain, respectively, whereas the latter two bands have transition dipole vectors perpendicular to the 1,4-axis.[32] The gain in intensity of the former signals and the concomitant decrease of the latter indicate a near upright position of the benzamidine headgroup.[21] Hence, the average tilt angles of the benzamidine group relative to the surface normal are small in

DOI: 10.1021/acscentsci.7b00412
ACS Cent. Sci. 2017, 3, 1198–1207

all layers (13−19°) with rSAM-**1** featuring the most upright groups (13°) (Supporting Information Table 1).

The position of the CH_2 asymmetric and symmetric stretch vibration (<2920 and 2850 cm^{-1} respectively for ordered SAMs) as well as the bandwidths in the low-frequency region of the spectra are informative of the order of the monolayer structure. Whereas rSAM-**1** features these bands at positions indicating liquid-like ordering (Figure 3B), the mixed rSAM-**1**+**2** appears more ordered (Figure 3C). However, as indicated by in situ ellipsometry (vide supra) and AFM (vide infra), **1** tends to form bilayered structures. The top layer in these assemblies is presumably less dense and/or less ordered than the underlying layer contributing in turn to the high frequency of this band. The stoichiometry of layer components of mixed SAMs has been deduced on the basis of component characteristic signals.[33] **2** features an ethylene glycol linker and a sialic acid headgroup with characteristic bands at 3345 cm^{-1} (amide N−H stretch, carboxylic acid, hydrogen bonded OH stretch), 1694 cm^{-1} (carboxylic acid, amide C═O stretch), 1431 cm^{-1} (carboxylic acid, C−OH bend), and 1115 cm^{-1} (aliphatic ethers, C−O−C stretch and secondary OH, C−C−O stretch). The normalized peak areas of these characteristic bands increase with increasing content of **2** (Supporting Information Figure 3, Supporting Information Table 4) showing that both amphiphiles coexist on the MHA-SAM. More precise conclusions in terms of stoichiometry and mixing cannot be drawn at this point. Instead we turned to AFM to obtain information concerning the lateral structure of the layers.

The AFM image of a SAM of MHA is shown in Figure 3E. This surface is relatively smooth with a roughness factor R_{RMS} of 0.21. The image obtained after the assembly of **1** on this surface in a pH 9 borate buffer revealed large (>50 nm) domains (Figure 3F) with a height of ca. 3 nm, in close agreement with the molecular length of **1**. Assuming a ca. 60% surface coverage (based on the height profile in Figure 3F) this should contribute roughly 2 nm to the layer thickness estimated using laterally averaging ellipsometry. However, in situ ellipsometry showed a layer thickness of 4.6 nm (see Supporting Information Table 1), which exceeds this value by more than 2.5 nm. From these observations we conclude that **1** is near perpendicularly oriented with respect to the surface (vide supra) and that the AFM height profile in this case depicts the less densely packed top layer. The bottom rSAM-**1** on the other hand appears densely packed. The domain structure prevails in the mixed rSAM (Figure 3G), which shows a larger height contrast compared to the rSAM of **1** alone. On the contrary, rSAM-**2** lacked domains and appeared as smooth as the SAM of MHA (Figure 3H). A static control for the rSAM-**2** surface, featuring covalently anchored sialic acid groups, was prepared by coupling **14** (Supporting Information Scheme 1) to a SAM of MHA. The resulting sialic acid SAM was characterized by FTIR, air ellipsometry, and AFM (Supporting Information Tables 1 and 5 and Supporting Information Figures 4 and 5). The results indicate the formation of a smooth, well ordered SAM with a sialic acid coverage of 27%, the latter somewhat lower than the estimated sialic acid coverage of rSAM-**2** of 40% (estimates based on the d_{rinse} values).

rSAM Interactions with Viral Proteins. In order to probe the rSAMs with respect to their affinity for the influenza lectin hemagglutinin (HA) we compared the adsorption of three proteins, the target lectin HA, concanavalin A (ConA) as a reference lectin, and human serum albumin (HSA), representing the predominant blood protein (Supporting Information Table 6). After assembly and rinse of rSAMs of **1** and **2** or a bare MHA-SAM in pH 8 buffer, protein was added (21 nM) and the film thickness followed in real time by ellipsometry until a stable reading was obtained. As seen in Figure 4A, the negatively charged MHA-SAM was resistant to HSA adsorption at this concentration whereas both lectins, ConA and HA, bound to reach approximately equal submonolayer thicknesses. The selectivity correlates to some extent with the isoelectric point p*I* of the proteins, which increases in the order HSA < ConA < HA (see Supporting Information Table 6). A different picture emerged when testing the two rSAMs prepared from **1** or **2**. Whereas rSAM-**2**, in accordance with the bare MHA-SAM, completely resisted HSA, the protein bound strongly to rSAM-**1** resulting in a 52 Å film. Moreover, rSAM-**2** displayed affinity for HA while showing a low cross-reactivity for the two other proteins and was thus the only surface displaying the targeted selectivity.

This result was confirmed by IRAS of rinsed surfaces subjected to the different proteins. As seen in Supporting Information Figure 6, the relative intensities of the amide I and II bands increased in the order HSA < ConA < HA. To prove that HA binding to rSAM-**2** was driven by the anticipated sialic acid−HA interactions we performed an additional control experiment. Mucin is an epithelial glycoprotein abundant in sialic acids.[34] Among other functions it acts as a virus barrier by binding with high affinity ($K_i = 2 \times 10^{-6}$ M) to HA.[35] By preincubating HA with mucin we expected the lectin binding sites to be masked and adsorption driven by sugar−lectin interactions to be suppressed. On the other hand, adsorption driven by nonspecific effects will not be affected in this experiment. Figure 4A demonstrates the anticipated effect. Hence, mucin effectively suppressed binding of HA to rSAM-**2** only, whereas it had no effect on binding to rSAM-**1** or the MHA-SAM. Moreover, mucin alone adsorbs nonspecifically to rSAM-**1** whereas rSAM-**2** appeared completely resistant vis-à-vis this protein.

Given the nonspecific binding exhibited by the rSAM-**1** (Figure 4A, Supporting Information Figure 7), we refrained from studies of mixed rSAM based on this amphiphile, but instead we decided to study the rSAM of pure **2** in more detail. Figure 4B shows the equilibrium binding curves obtained after titrating freshly rinsed rSAM-**2** with HA, ConA, and HSA, and Supporting Information Figure 8 shows the ellipsometric trace during a full cycle of titration and pH induced regeneration. This experiment fully confirms the functional properties of the glycan rSAM. Titration with HA resulted in a binding curve showing a steep initial portion followed by a clear saturation at concentrations exceeding 20 nM. This curve was best fitted with the Hill equation resulting in an overall equilibrium dissociation constant, K_d^{multi}, of 5.1 nM and an estimated detection limit of 0.84 nM (Supporting Information Table 7). These results contrasted with the behavior of rSAM-**1** and the SAM of MHA. The corresponding binding curves were shallower and did not reach saturation within the investigated concentration interval (Supporting Information Figure 7).

The weakly sigmoidal shape is in agreement with the glycan clustering effect and multivalent binding. The ConA binding curve however was shallow and showed no evidence of cooperativity, nor was saturation reached within the probed concentration interval. Hence, the results agree with the relative glycan specificity of the two lectins. Finally, as indicated by the lack of HSA binding, the surface appeared resistant to nonspecific binding of plasma proteins. Remarkably, the substrate could be used repeatedly by carrying out a pH induced regeneration (Supporting Information Figure 8). The complete removal of the

DOI: 10.1021/acscentsci.7b00412
ACS Cent. Sci. 2017, 3, 1198−1207

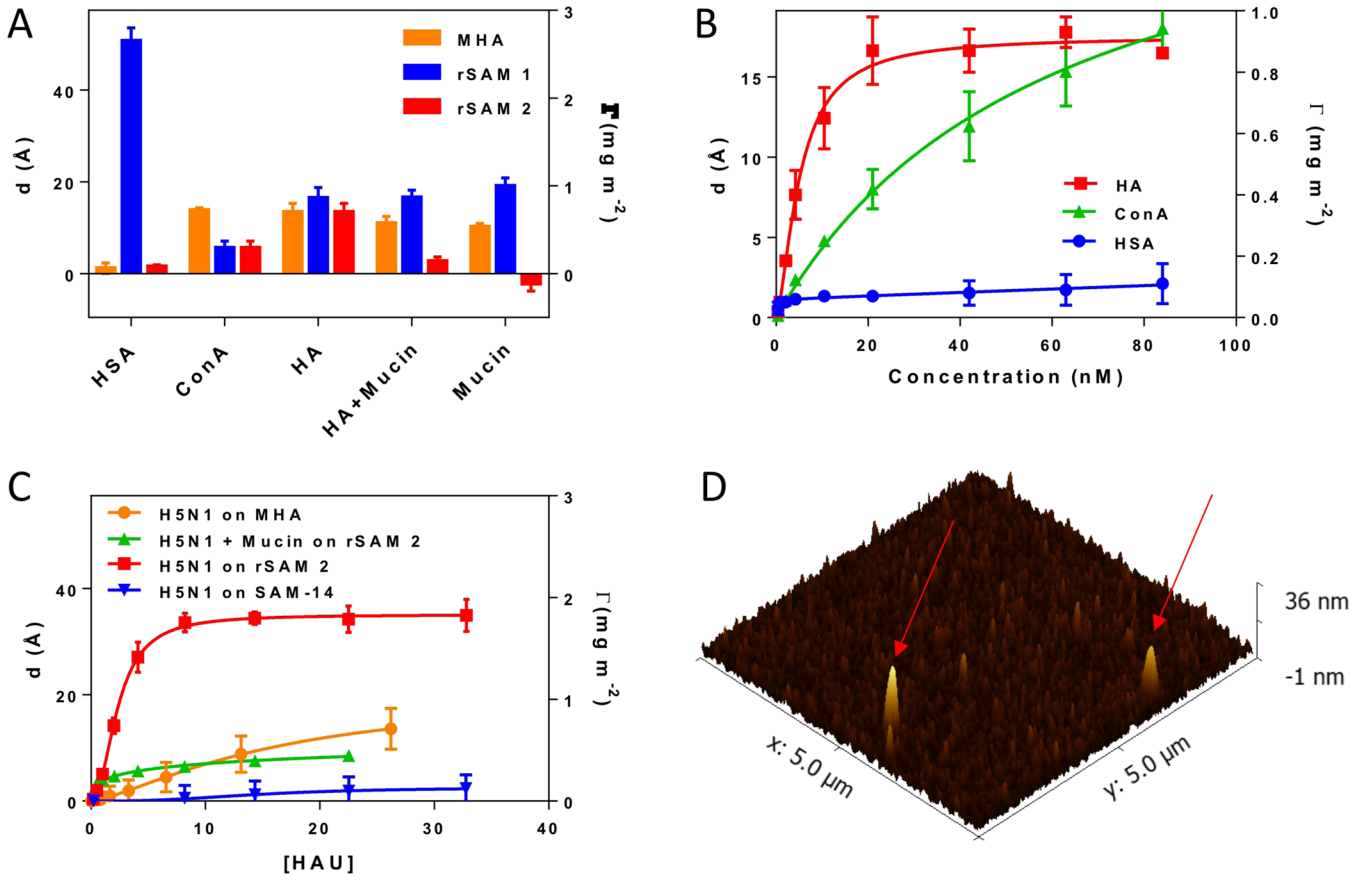

Figure 4. Film thickness, *d*, and adsorbed amount, Γ, estimated by ellipsometry for (A) a bare MHA-SAM on gold (orange bars), rSAM-**1** (blue bars), or rSAM-**2** (red bars) after exposure to solutions of HA, ConA, HSA, HA preincubated with mucin, or 0.005% (w/v) mucin until stable Δ and Ψ values were obtained or for a maximum duration of 5000 s (whichever came first); (B) rSAM-**2** upon addition of incremental amounts of HA (red squares), ConA (green triangles), or HSA (blue circles); and (C) MHA-SAM (orange circles) or rSAM-**2** (red squares) or SAM-**14** (blue triangles) upon addition of deactivated influenza virus H5N1 (0.20−33 HAU) and rSAM **2** upon addition of deactivated influenza virus H5N1 preincubated with mucin (green triangles). Equilibrium dissociation constants, K_d, maximum specific binding, Γ_{max}, and the Hill slope, *h*, are tabulated in Supporting Information Table 7. (D) Surface topography of an rSAM of **2** on MHA modified gold after exposure to deactivated H5N1 (14 HAU) followed by rinsing with pH 8 HEPES buffer. Identified virus particles are indicated by arrows.

rSAM was confirmed by ellipsometry, IRAS, and contact angle measurements (Supporting Information Figure 9).

rSAM Interaction with Influenza Virus H5N1. As examplified by the "bird flu", certain strains of the H5N1 influenza A virus subtype can be highly pathogenic, and its pathogenicity is expected to rise. In order to probe the affinity of our dynamic rSAMs for this virus we subjected them to inactivated virus particles provided by the World Health Organization (WHO). We started by carrying out a titration experiment identical to the one performed for the proteins (Figure 4C) using three different surfaces, rSAM-**2**, SAM-**14** featuring covalently attached sialic acids, and the anchoring MHA-SAM.

In analogy with the HA binding results (vide supra), the virus bound strongly to rSAM-**2** (Supporting Information Figure 10) with a clear cooperative binding behavior while showing very weak affinity for SAM-**14** and the underlying MHA-SAM. Fitting the curve with the Hill equation resulted in a K_d^{multi} of 2.3×10^{-13} M and a detection limit of 0.5 HAU (46 fM) (Supporting Information Figure 11), the latter corresponding to a mass sensitivity (assuming a virus molecular weight of 2.5×10^8 g/mol)[36] of ca. 11 µg/L (Supporting Information Table 7). Adsorption of the virus was effectively suppressed by the mucin induced masking of HA (Figure 4C).

In order to assess the influence of potential errors due to nonequilibrium binding we also performed a kinetic multicycle interaction analysis. The rate constants for virus adsorption and desorption were calculated from the adsorption and desorption rate profiles as described in the Supporting Information (Supporting Information section 1.7 and Figure 12). The dissociation constants, K_d, determined by this method (Supporting Information Table 8) were in good agreement with the equilibrium analysis.

The high affinity displayed by rSAM-**2** stand in striking contrast to the weak virus adsorption on SAM-**14**. The two SAMs feature nearly identical tethers but different ligand densities (40% and 27% respectively). Although this makes an unambiguous comparison difficult, it should be noted that mixed thiol SAMs with lower ligand densities typically show higher lectin/virus affinities. Hence, surfaces with less than 20% of the head groups being glycans are more effective binders whereas binding drops with increasing ligand density.[8] Moreover we note that comparable sialic acid modified SAMs also display low affinity, e.g., in the µM range toward hemagglutinin.[37] All in all, this strongly indicates that dynamic interactions in rSAMs play an important role in enhancing influenza virus detection.

AFM images recorded for a rinsed rSAM-**2** exposed to the virus are shown in Figure 4D. The virus particles could be

DOI: 10.1021/acscentsci.7b00412
ACS Cent. Sci. 2017, 3, 1198−1207

discerned as spikes with a height of ca. 40 nm that were absent in images of rSAM-**2** prior to virus exposure (Supporting Information Figure 13). The surface roughness after virus exposure (R_a = 2.3 nm) agreed with results reported for a glycan modified thiol SAM.[8] pH-induced restoration of the MHA-SAM was proven by IRAS and contact angle measurements of the surface prior to and post acidification (Supporting Information Figure 9). Hence the MHA-SAM was stable and the sensor could be reused several times.

Optimization of Ligand Density and Presentation. We recall that the above results were obtained for an rSAM of **2** only and that efforts to use mixed rSAMs were hampered by excessive nonspecific binding on rSAM-**1**. We therefore set out to prepare more protein resistant surfaces based on oligoethylene glycol (EG) terminated rSAMs and accordingly to optimize the sialic acid tether length. As shown in Figure 5 a careful tuning of ligand

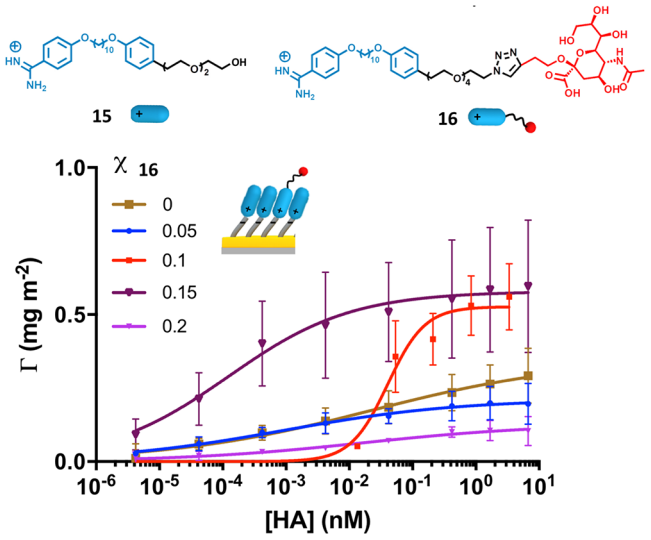

Figure 5. Hemagglutinin binding isotherms of rSAMs formed with varying density of EG4-sialic acid **16** (χ_{16}) in mixed rSAMs of **15** and **16**.

presentation and ligand density leads to a strongly enhanced affinity for hemagglutinin (HA). Based on four EG repeats in the sialic acid tether as in **16** and two repeats in the OH-terminated amidine **15**, the affinity for HA peaks at rather low ligand densities. For a surface prepared from 15% sialic acid amidine **16** it can be seen that the affinity has increased dramatically, resulting in a K_d^{multi} of 1.2×10^{-13} M, i.e., four orders of magnitude lower K_d than the nM affinity reported for rSAM-**2**. The latter is nevertheless on a par with the best binders reported to date. These results are also in agreement with literature results, where optimal glycan densities are typically in the same range as we report here.[8]

Lateral Dynamics of Layer Components. As noted above, the high affinities displayed by the rSAMs likely stem from the dynamic nature of the films. To back up this hypothesis, we have used fluorescence recovery after photobleaching (FRAP) as a means to study monolayer fluidity. As shown in Supporting Information Figure 14, dye doped rSAMs of **15** on quartz display fluorescence recovery in a time span similar to that observed for supported lipid bilayers.[38] This clearly suggests layer dynamics to be the major cause of the enhanced affinities observed using the rSAM platform.

Comparison with Literature. As a means to compare the affinity of our assemblies with literature, we have summarized the

Table 1. Comparison of Monosaccharide Based Sensors and Inhibitors

lectin binder	target	K_d (K_i)[a] (M)	ref
rSAM-**2**	HA	1.5×10^{-8}	this work
rSAM **15**+**16**	HA	3.6×10^{-13}	this work
rSAM-**2**	H5N1	3.4×10^{-10}	this work
α-methyl sialoside	HA	2.0×10^{-3}	39
trivalent inhibitor	HA	1.3×10^{-6}	14
linear polymers[b]	H3N2	$<10^{-8}$	15
gold nanoparticles	H3N2	(10^{-9})	18
polymerized bilayers	H3N2	10^{-9} [c]	40
liposomes[d]	H3N2	(2×10^{-8})	17

[a] K_d = dissociation constant per SA or HA monomer unit. Inhibition constants, K_i, are given in parentheses. [b] K_d tabulated are based on the best performing polymers. [c] Estimated graphically based on reported binding curve. [d] Polymerized liposomes reported by Charych et al.[26] show a limit of detection of ca. 4 HAU/mL.

affinity data of a series of assemblies based on α-sialoside groups (Table 1) and calculated the equilibrium dissociation constants, K_d, per sialic acid or monomeric HA. Making the assumption that each trimeric hemagglutinin has 3 sialic acid binding sites, the K_d of our system toward HA was estimated to 1.5×10^{-8} M for rSAM-**2** and 3.6×10^{-13} M for rSAM**15**+**16** per monomeric hemagglutinin, HA_{mono} basis.[11] Likewise, assuming each virus to contain 1500 sialic acid binding sites, the K_d toward H5N1 was estimated to 3.4×10^{-10} M per monomeric hemagglutinin. To the best of our knowledge, α-sialoside glycopolymer has the highest reported affinity toward influenza viruses with an inhibition constant, K_i, of 10^{-10} M and a dissociation constant $K_d < 10^{-8}$ M per sialic acid unit. The tightest inhibitor for hemagglutinin is however a small molecule trivalent sialic acid with a K_d of 1.3×10^{-6} M. A comparison with other dynamic platforms such as liposomes and lipid bilayers is of particular relevance. These feature fluid bilayers where the sialic acids can diffuse laterally, in this respect ressembling the dynamic rSAM concept. An inhibition constant K_i of 2×10^{-8} M was reported for a liposome based multivalent inhibitor whereas polymerized liposomes bound influenza virus with a limit of detection of 4 HAU. Dissociation constants in the range $K_d^{multi} = 10^{-10}$–10^{-11} M were measured for H5N3 and H3N2 interacting with gangliosides (with intrinsically higher lectin affinity) in lipid bilayers.[36] Although different techniques may have been used to determine the K_d's, we can conclude that the affinity of our sialic acid rSAMs is on par with or exceeds that of the most potent binders reported.

CONCLUSIONS

We have demonstrated a new generic supramolecular concept for multivalent recognition and proven its benefits for enhancing recognition in affinity biosensors. Our results consistently show an overall enhanced affinity for both lectin and virus with respect to previous reports, which we attribute to a unique lipid bilayer like ligand adaptability. Another advantage of this glycan-based sensor is the simple architecture. Only three components are used to set up this sensor for detection. It can be built up in two immersion steps and is ready for detection with the significant advantage of substrate reusability. Further work will address the specificity of the sensor in terms of virus subtype recognition and extension of the operational pH range. Moreover, we will show in forthcoming reports the generic nature of the rSAM concept to boost biosensor affinity and restorability.

DOI: 10.1021/acscentsci.7b00412
ACS Cent. Sci. 2017, 3, 1198–1207

METHODS

Preparation of Protein and Virus Solutions. Influenza A H5N1 (A/Anhui/2005) hemagglutinin (HA) was purchased from Sino Biological Inc. Concanavalin A (ConA), human serum albumin (HSA), and mucin from porcine stomach (type III, bound sialic acid 0.5−1.5%) were obtained from Sigma-Aldrich. Stock solutions of HA, ConA, HSA (4.2 μM), and mucin (1% w/v) were prepared in Milli-Q water or pH 8 HEPES buffer (0.01 M) and stored at −80 °C prior to usage. Influenza A (H5N1) Surveillance Antigen, BPL-Inactivated Influenza A Virus, A/Anhui/01/2005(H5N1)-PR8-IBCDC-RG6, FR-918, was generously provided through the Influenza Reagent Resource, Influenza Division, WHO Collaborating Center for Surveillance, Epidemiology and Control of Influenza, Centers for Disease Control and Prevention, Atlanta, GA, USA, and was used without further treatment. The hemagglutination titer of the influenza virus was 512 HAU, and the estimated concentration (mol L^{-1}) was determined using eq 1.

$$\text{concentration of virus (mol L}^{-1}) = \frac{CB \times 10^3}{L} \quad (1)$$

where C is concentration of the virus in HAU, [HAU] mL^{-1}, B is the estimated number of virus particles per HAU, 5.5×10^7 units HAU^{-1},[41] and L is the Avogadro constant, 6.022×10^{23} units mol^{-1}. For the inhibitory studies, the solutions were prepared by shaking H5N1 (512 HAU) or HA (4.2 μM) with equal volume of 1% mucin in pH 8 HEPES buffer for a minimum of 30 min prior to absorption studies.

Adsorption Experiments. The adsorption process of amidine, protein, or virus was monitored using in situ null ellipsometry. The instrument used was a Rudolph thin film ellipsometer (type 43603-200E, Rudolph Research, USA) using an angle of incidence of 68° and automated according to Cuypers et al.[42] The light source was a xenon lamp, filtered to λ = 442.9 nm. The thiol SAMs prepared as described in the Supporting Information were immersed vertically into an ellipsometric quartz cuvette with ordinary microscopic cover glass windows containing 5 mL of sodium borate buffer (0.01 M, pH 9.0, prepared from boric acid). The cuvette was thermostated to 25 °C and equipped with a magnetic stirrer at constant stirring rate of 350 rpm. Before each measurement, the refractive index of the MHA gold substrate was determined by a 4-zone surface calibration in pH 9 HEPES solution.

Amidine Addition. After a stable baseline was obtained, 100 μL of stock solution containing **1**, **2**, or a mixture of **1** and **2** (χ = 0.2) (2.5 mM) was added to the cuvette. Kinetics data was collected until stabilization or for a maximum duration of 5000 s. The system was then rinsed with pH 8 HEPES buffer for a maximum of 1000 s (11 mL min^{-1}) in a continuous system. The surface was later allowed to stabilize until steady state or 5000 s (whichever came first).

Protein Addition. After the adsorption of rSAMs (vide supra), the selectivity of the surfaces was tested by measuring the adsorption of 21 nM or 5.3 nM (ConA) solutions (HEPES buffer, 0.01 M, pH 8) of the proteins HA, ConA, and HSA by in situ ellipsometry. Binding curves were recorded by adding incremental amounts of the respective protein (0.42−84 nM) or virus (0.2−33 HAU) to the cuvette and monitoring the adsorption by in situ ellipsometry. The additions were made every 2000 s using the respective stock solution prepared as described above. The surfaces were subsequently either regenerated by 0.1 M HCl or blown dry using nitrogen and subjected to further characterization by IRAS, contact angle, or AFM.

Calculations of Thickness and Adsorbed Amounts. A homogeneous 3-layer model was used to determine the average thickness, d, and adsorbed amount, Γ, from the ellipsometric data according to eq 2.[43,44]

$$\Gamma = d_A \frac{n - n_0}{dn/dc} \quad (2)$$

where d_A is the thickness of the adsorbed layer, n is the refractive index of the molecules, n_0 is the refractive index of the ambient, and dn/dc is the refractive index increment for the molecules in the layer. The thickness of the rSAMs was calculated using a homogeneous 3 layer model (MHA Au−rSAM−buffer solution) with assumed refractive index of 1.45 and 1.34 for rSAMs and ambient, respectively. The ellipsometric determined thickness of rSAMs using this model has been previously verified using neutron reflectivity.[20] Refractive index increment, dn/dc, of 0.22 mg mL^{-1} was used to determine the amount of rSAMs adsorbed.[45] Relative adsorbed protein thickness was calculated based on a homogeneous 3-layer model (rSAMs−protein−buffer solution) with refractive index of 1.45 for protein. It assumed that minimum penetration or exchange occurred between the interface and analyte during the adsorption process. The thicknesses obtained are relative values to describe trends in the protein adsorption.[46] A refractive index increment, dn/dc, of 0.19 mg mL^{-1} was used to determine the adsorbed amount of protein.[47]

Statistical Methods. Equilibrium binding analysis based on successive injections (single cycle measurement)[48] was used to determine the dissociation constant, K_d, limiting adsorbed amount, Γ_{max}, and Hill slope, h. The technique requires a way to accurately determine the steady state value of thickness, d, and adsorbed amount, Γ. We considered the latter to have reached a plateau within 2000 s. If this was not the case, the curves were extrapolated to steady state values by nonlinear curve fitting.

The limit of detection (LoD) was estimated as the concentration producing a signal corresponding to a minimum of three times the standard deviation (SD) of the blank signal. The binding curves were fitted to the Hill equation using Graphpad Prism v7.0. Error bars are standard error of the mean (SEM) describing the range between the values obtained unless stated otherwise. All values are averages of a minimum of two experiments on different substrates. Raw plots and details of fitting are shown in the Supporting Information. Molecular length of the compounds was estimated after minimizing the energy of the corresponding compound using molecular mechanics calculations with the MM2 force field (ChemDraw 3D, CambridgeSoft).

ASSOCIATED CONTENT

Supporting Information

The Supporting Information is available free of charge on the ACS Publications website at DOI: 10.1021/acscentsci.7b00412.

Experimental details and characterization data including compound synthesis and substrate and SAM and rSAM preparation and characterization (PDF)

AUTHOR INFORMATION

Corresponding Author

*E-mail: borje.sellergren@mah.se.

ORCID

Börje Sellergren: 0000-0002-2392-3305

DOI: 10.1021/acscentsci.7b00412
ACS Cent. Sci. 2017, 3, 1198−1207

Notes

The authors declare no competing financial interest.

■ ACKNOWLEDGMENTS

This work was supported by grants from the Swedish Research Council (Contract No. C0296601), Deutsche Forschungsgemeinschaft (Project Se 777/2-5), the Crafoord Foundation (grant number 20150923) and the Gustaf Th. Ohlsson Foundation. The gift of influenza virus from Influenza Reagent Resource is gratefully acknowledged. We are grateful to Thomas Ederth, Linköping University, and to Javier Soutres (Malmö University) for assistance with the FRAP and AFM experiments respectively and for helpful discussions. Kishore Kumar Jagadeesan (Lund University), Guoqing Pan, Eglė Malcaitė, Eglė Pakalnytė, Vivek Chaturverdi, and Madhuri Nagabhushanam, Malmö University, are acknowledged for experimental assistance.

■ REFERENCES

(1) Peiris, J. S. M.; de Jong, M. D.; Guan, Y. Avian Influenza Virus (H5N1): a Threat to Human Health. *Clin. Microbiol. Rev.* **2007**, *20*, 243−267.

(2) Taubenberger, J. K.; Morens, D. M. Influenza Viruses: Breaking All the Rules. *mBio* **2013**, *4* (4), e00365-13.

(3) Eisfeld, A. J.; Neumann, G.; Kawaoka, Y. Influenza A virus isolation, culture and identification. *Nat. Protoc.* **2014**, *9*, 2663−2681.

(4) De Clercq, E.; Li, G. Approved Antiviral Drugs over the Past 50 Years. *Clin. Microbiol. Rev.* **2016**, *29*, 695−747.

(5) Spevak, W.; Nagy, J. O.; Charych, D. H. Molecular assemblies of functionalized polydiacetylenes. *Adv. Mater.* **1995**, *7*, 85−89.

(6) Gopinath, S. C. B.; et al. Sensing strategies for influenza surveillance. *Biosens. Bioelectron.* **2014**, *61*, 357−369.

(7) Wicklein, B.; et al. Biomimetic Architectures for the Impedimetric Discrimination of Influenza Virus Phenotypes. *Adv. Funct. Mater.* **2013**, *23*, 254−262.

(8) Hushegyi, A.; et al. Ultrasensitive detection of influenza viruses with a glycan-based impedimetric biosensor. *Biosens. Bioelectron.* **2016**, *79*, 644−649.

(9) Su, L.-C.; et al. Rapid and Highly Sensitive Method for Influenza A (H1N1) Virus Detection. *Anal. Chem.* **2012**, *84*, 3914−3920.

(10) Hideshima, S.; et al. Attomolar Detection of Influenza A Virus Hemagglutinin Human H1 and Avian H5 Using Glycan-Blotted Field Effect Transistor Biosensor. *Anal. Chem.* **2013**, *85*, 5641−5644.

(11) Mammen, M.; Choi, S.-K.; Whitesides, G. M. Polyvalent Interactions in Biological Systems: Implications for Design and Use of Multivalent Ligands and Inhibitors. *Angew. Chem., Int. Ed.* **1998**, *37*, 2754−2794.

(12) Bhatia, S.; Camacho, L. C.; Haag, R. Pathogen Inhibition by Multivalent Ligand Architectures. *J. Am. Chem. Soc.* **2016**, *138*, 8654−8666.

(13) Carlescu, I.; Scutaru, D.; Popa, M.; Uglea, C. V. Synthetic sialic-acid-containing polyvalent antiviral inhibitors. *Med. Chem. Res.* **2009**, *18*, 477−494.

(14) Waldmann, M.; et al. A Nanomolar Multivalent Ligand as Entry Inhibitor of the Hemagglutinin of Avian Influenza. *J. Am. Chem. Soc.* **2014**, *136*, 783−788.

(15) Sigal, G. B.; Mammen, M.; Dahmann, G.; Whitesides, G. M. Polyacrylamides Bearing Pendant α-Sialoside Groups Strongly Inhibit Agglutination of Erythrocytes by Influenza Virus: The Strong Inhibition Reflects Enhanced Binding through Cooperative Polyvalent Interactions. *J. Am. Chem. Soc.* **1996**, *118*, 3789−3800.

(16) Shen, L.; Wang, Y.; Lin, C.-I.; Lin, H.-W.; Guo, A.; Zhu, X. Y. Membrane Environment Can Enhance the Interaction of Glycan Binding Protein to Cell Surface Glycan Receptors. *ACS Chem. Biol.* **2014**, *9*, 1877.

(17) Kingery-Wood, J. E.; Williams, K. W.; Sigal, G. B.; Whitesides, G. M. The agglutination of erythrocytes by influenza virus is strongly inhibited by liposomes incorporating an analog of sialyl gangliosides. *J. Am. Chem. Soc.* **1992**, *114*, 7303−7305.

(18) Papp, I.; et al. Inhibition of Influenza Virus Infection by Multivalent Sialic-Acid-Functionalized Gold Nanoparticles. *Small* **2010**, *6*, 2900−2906.

(19) Castellana, E. T.; Cremer, P. S. Solid supported lipid bilayers: From biophysical studies to sensor design. *Surf. Sci. Rep.* **2006**, *61*, 429−443.

(20) Auer, F.; et al. Switchable assembly of stable, ordered molecular layers. *Chem. - Eur. J.* **1999**, *5*, 1150−1159.

(21) Auer, F.; Nelles, G.; Sellergren, B. Odd−Even Chain Length-Dependent Order in pH-Switchable Self-Assembled Layers. *Chem. - Eur. J.* **2004**, *10*, 3232−3240.

(22) Sellergren, B.; Auer, F.; Arnebrant, T. Selective binding of DNA oligonucleotides to switchable selfassembled molecular layers. *Chem. Commun.* **1999**, 2001−2002.

(23) Sellergren, B.; Swietlow, A.; Arnebrant, T.; Unger, K. Consecutive Selective Adsorption of Pentamidine and Phosphate Biomolecules on a Self - Assembled Layer: Reversible Formation of a Chemically Selective Coating. *Anal. Chem.* **1996**, *68*, 402−407.

(24) Casalini, S.; Bortolotti, C. A.; Leonardi, F.; Biscarini, F. Self-assembled monolayers in organic electronics. *Chem. Soc. Rev.* **2017**, *46*, 40−71.

(25) Mrksich, M.; Whitesides, G. M. Using self - assembled monolayers to understand the interactions of man-made surfaces with proteins and cells. *Annu. Rev. Biophys. Biomol. Struct.* **1996**, *25*, 55−78.

(26) Reichert, A.; Nagy, J. O.; Spevak, W.; Charych, D. Polydiacetylene Liposomes Functionalized with Sialic Acid Bind and Colorimetrically Detect Influenza Virus. *J. Am. Chem. Soc.* **1995**, *117*, 829−830.

(27) Rostovtsev, V. V.; Green, L. G.; Fokin, V. V.; Sharpless, K. B. A Stepwise Huisgen Cycloaddition Process: Copper(I)-Catalyzed Regioselective "Ligation" of Azides and Terminal Alkynes. *Angew. Chem., Int. Ed.* **2002**, *41*, 2596−2599.

(28) Tidwell, R. R.; Jones, S. K.; Geratz, J. D.; Ohemeng, K. A.; Cory, M.; Hall, J. E. Analogues of 1,5-bis(4-amidinophenoxy)pentane (pentamidine) in the treatment of experimental Pnemocystis carinii pneumonia. *J. Med. Chem.* **1990**, *33*, 1252−1257.

(29) Deng, L.; Norberg, O.; Uppalapati, S.; Yan, M.; Ramstrom, O. Stereoselective synthesis of light-activatable perfluorophenylazide-conjugated carbohydrates for glycoarray fabrication and evaluation of structural effects on protein binding by SPR imaging. *Org. Biomol. Chem.* **2011**, *9*, 3188−3198.

(30) Deng, J.; Sheng, Z.; Zhou, K.; Duan, M.; Yu, C.-Y.; Jiang, L. Construction of Effective Receptor for Recognition of Avian Influenza H5N1 Protein HA1 by Assembly of Monohead Glycolipids on Polydiacetylene Vesicle Surface. *Bioconjugate Chemistry* **2009**, *20*, 533.

(31) Smith, E. L.; Alves, C. A.; Anderegg, J. W.; Porter, M. D.; Siperko, L. M. Deposition of metal overlayers at end-group-functionalized thiolate monolayers adsorbed at gold. 1. Surface and interfacial chemical characterization of deposited copper overlayers at carboxylic acid-terminated structures. *Langmuir* **1992**, *8*, 2707−2714.

(32) Chang, S.-C.; Chao, I.; Tao, Y.-T. Structures of selfassembled monolayers of aromatic derivatized thiols on evaporated gold and silver surfaces: Implication on packing mechanism. *J. Am. Chem. Soc.* **1994**, *116*, 6792−6805.

(33) Kang, J. F.; Ulman, A.; Liao, S.; Jordan, R. Mixed Self-Assembled Monolayers of Highly Polar Rigid Biphenyl Thiols. *Langmuir* **1999**, *15*, 2095−2098.

(34) Gaunitz, S.; Liu, J.; Nilsson, A.; Karlsson, N.; Holgersson, J. Avian influenza H5 hemagglutinin binds with high avidity to sialic acid on different O-linked core structures on mucin-type fusion proteins. *Glycoconjugate J.* **2014**, *31*, 145−159.

(35) Tang, S.; et al. Antiviral Agents from Multivalent Presentation of Sialyl Oligosaccharides on Brush Polymers. *ACS Macro Lett.* **2016**, *5*, 413−418.

(36) Hidari, K. I. P. J.; Shimada, S.; Suzuki, Y.; Suzuki, T. Binding kinetics of influenza viruses to sialic acid-containing carbohydrates. *Glycoconjugate J.* **2007**, *24*, 583−590.

DOI: 10.1021/acscentsci.7b00412
ACS Cent. Sci. 2017, 3, 1198−1207

(37) Diltemiz, S. E.; Ersöz, A.; Hür, D.; Keçili, R.; Say, R. 4-Aminophenyl boronic acid modified gold platforms for influenza diagnosis. *Mater. Sci. Eng., C* **2013**, *33*, 824−830.
(38) Deng, Y.; et al. Fluidic and Air-Stable Supported Lipid Bilayer and Cell-Mimicking Microarrays. *J. Am. Chem. Soc.* **2008**, *130*, 6267−6271.
(39) Sauter, N. K.; et al. Hemagglutinins from two influenza virus variants bind to sialic acid derivatives with millimolar dissociation constants: a 500-MHz proton nuclear magnetic resonance study. *Biochemistry* **1989**, *28*, 8388−8396.
(40) Charych, D. H.; Nagy, J. O.; Spevak, W.; Bednarski, M. D. Direct colorimetric detection of a receptor-ligand interaction by a polymerized bilayer assembly. *Science* **1993**, *261*, 585−588.
(41) Kramberger, P.; Ciringer, M.; Štrancar, A.; Peterka, M. Evaluation of nanoparticle tracking analysis for total virus particle determination. *Virol. J.* **2012**, *9*, 265.
(42) Cuypers, P. A.; et al. The adsorption of prothrombin to phosphatidylserine multilayers quantitated by ellipsometry. *J. Biol. Chem.* **1983**, *258*, 2426−2431.
(43) De Feijter, J. A.; Benjamins, J.; Veer, F. A. Ellipsometry as a tool to study the adsorption behavior of synthetic and biopolymers at the air−water interface. *Biopolymers* **1978**, *17*, 1759−1772.
(44) McCrackin, F.; Passaglia, E.; Stromberg, R.; Steinberg, H. Measurement of the thickness and refractive index of very thin films and the optical properties of surfaces by ellipsometry. *J. Res. Natl. Bur. Stand., Sect. A* **1963**, *67A*, 363−377.
(45) Davis, T. M.; Wilson, W. D. Determination of the Refractive Index Increments of Small Molecules for Correction of Surface Plasmon Resonance Data. *Anal. Biochem.* **2000**, *284*, 348−353.
(46) Prime, K. L.; Whitesides, G. M. Adsorption of proteins onto surfaces containing end-attached oligo(ethylene oxide): a model system using self-assembled monolayers. *J. Am. Chem. Soc.* **1993**, *115*, 10714−10721.
(47) Tengvall, P.; Lundström, I.; Liedberg, B. Protein adsorption studies on model organic surfaces: an ellipsometric and infrared spectroscopic approach. *Biomaterials* **1998**, *19*, 407−422.
(48) Myszka, D. G.; Jonsen, M. D.; Graves, B. J. Equilibrium Analysis of High Affinity Interactions Using BIACORE. *Anal. Biochem.* **1998**, *265*, 326−330.

DOI: 10.1021/acscentsci.7b00412
ACS Cent. Sci. 2017, 3, 1198−1207